SEDIMENTOLOGY the journal of the International Association of Sedimentologists

Sedimentology (2017) **64**, 987–1004 doi: 10.1111/sed.12338

Estimating the settling velocity of bioclastic sediment using common grain-size analysis techniques

MICHAEL V. W. CUTTLER*, RYAN J. LOWE*, JAMES L. FALTER* and DANIEL BUSCOMBE†

**ARC Centre of Excellence for Coral Reef Studies, UWA Oceans Institute, School of Earth and Environment, The University of Western Australia (M004), 35 Stirling Highway, Crawley, WA 6009, Australia (E-mail: michael.cuttler@research.uwa.edu.au)*

†U.S. Geological Survey, Southwest Biological Center, Grand Canyon Monitoring and Research Center, 2255 N. Gemini Drive, Flagstaff, AZ 86001, USA

Associate Editor – Subhasish Dey

ABSTRACT

Most techniques for estimating settling velocities of natural particles have been developed for siliciclastic sediments. Therefore, to understand how these techniques apply to bioclastic environments, measured settling velocities of bioclastic sedimentary deposits sampled from a nearshore fringing reef in Western Australia were compared with settling velocities calculated using results from several common grain-size analysis techniques (sieve, laser diffraction and image analysis) and established models. The effects of sediment density and shape were also examined using a range of density values and three different models of settling velocity. Sediment density was found to have a significant effect on calculated settling velocity, causing a range in normalized root-mean-square error of up to 28%, depending upon settling velocity model and grain-size method. Accounting for particle shape reduced errors in predicted settling velocity by 3% to 6% and removed any velocity-dependent bias, which is particularly important for the fastest settling fractions. When shape was accounted for and measured density was used, normalized root-mean-square errors were 4%, 10% and 18% for laser diffraction, sieve and image analysis, respectively. The results of this study show that established models of settling velocity that account for particle shape can be used to estimate settling velocity of irregularly shaped, sand-sized bioclastic sediments from sieve, laser diffraction, or image analysis-derived measures of grain size with a limited amount of error. Collectively, these findings will allow for grain-size data measured with different methods to be accurately converted to settling velocity for comparison. This will facilitate greater understanding of the hydraulic properties of bioclastic sediment which can help to increase our general knowledge of sediment dynamics in these environments.

Keywords Bioclastic sediment, grain size, image analysis, laser diffraction, settling tube, settling velocity, sieve.

INTRODUCTION

Settling velocity in water is a fundamental physical property of sediments, which can be used to understand how sediment is entrained, transported and deposited in marine environments (Miller *et al.*, 1977; Komar & Clemens, 1986; Le Roux, 2002; Paphitis *et al.*, 2002). Settling velocity is key to understanding both the hydrodynamic properties of bed sediment, and

thus the transport mode and/or entrainment thresholds (Shields, 1936; Rouse, 1937), as well as sedimentary plume dynamics, where settling velocity determines sediment fallout times and advection length scales (Syvitski *et al.*, 1988). Furthermore, this can be of particular importance in environments such as estuaries, where deposition of suspended material can lead to harmful build-ups of heavy metals (Birch & Taylor, 1999); or in coral reefs, where increased turbidity can limit light availability (Storlazzi *et al.*, 2015) and lead to coral stress and/or mortality (Rogers, 1990).

The settling velocity of a particle is determined by its size, shape and density. These variables have been empirically related for straightforward conversion from grain diameter, a commonly measured parameter, to settling velocity (Gibbs *et al.*, 1971; Dietrich, 1982; Le Roux, 1992, 2002; Cheng, 1997; Ferguson & Church, 2004). Although each model accounts for particle size and density, each has a different treatment of particle shape. For example, the Gibbs *et al.* (1971) relationship makes no correction for grain shape, thus accounting only for sediment density and size; the Ferguson & Church (2004) equation uses two constants that are related to grain shape; and Dietrich (1982) explicitly accounts for grain shape through the Corey (1949) shape factor (CSF) and grain roundness through the Powers (1953) roundness index (PRI).

These equations have been developed and tested principally for siliciclastic sediments; however, it remains unclear how accurate these equations are when applied to bioclastic sediment that is typically highly irregular in shape and density. Bioclastic sediment is derived from the physical and chemical breakdown of biogenic structures (for example, coral reefs) and the death of organisms (for example, foraminifera, molluscs, *Halimeda*). These sediment sources have a direct influence on particle morphologies, sizes and densities present in the sediment pool because organisms build skeletons with specific porosities, and therefore densities, and break down into characteristic shapes and sizes (Sorby, 1879; Perry *et al.*, 2011). For example, *Halimeda* and mollusc fragments tend to form plate-like particles, urchin spines form rod-like particles, foraminifera generally form disc-like particles, and most corals and coralline algae form irregular, block-like particles (Maiklem, 1968; Braithwaite, 1973). Because these irregularities make it difficult to derive a characteristic grain diameter for bioclastic deposits using common grain-size techniques, settling velocity has been suggested to be a more meaningful metric for interpretation of bioclastic sedimentary deposits (Kench & McLean, 1996). Although settling tube is the primary method for analysing settling velocity of bulk samples, this analysis can be resource intensive and not all laboratories have this equipment; therefore, other common grain-size methods are frequently applied to study bioclastic environments (Folk & Robles, 1964; Harney *et al.*, 2000; Larcombe *et al.*, 2001). Thus, there is a clear need to understand how accurately results from common grain-size techniques can be converted to settling velocities using established empirical models.

Common methods to measure grain-size distributions (GSDs) include sieves, laser diffraction and image analysis. Sieve analysis involves sorting sediment particles through a series of square-mesh screens, whereby it is assumed that the particles are spherical with a diameter corresponding to the length of the side of the square sieve openings (Komar & Cui, 1984). As particles become more irregular (i.e. less spherical), the length of a grain's intermediate (second largest) axis relative to the length of the diagonal of the square sieve opening determines passage of the grain through the sieve (Rittenhouse, 1943; Komar & Cui, 1984). Laser diffraction measures the 'nominal' diameter of a grain, or the diameter of a sphere with the same volume and of the same material as the measured grain, based on the forward scattering of a parallel beam of monochromatic light, with scatter angle and intensity related to grain size by a specific optical model (Cheetham *et al.*, 2008). Thus, like sieving, grain sizes derived from laser diffraction provide idealized, scalar value representations of the actual three-dimensional irregularity of natural sediments. Image analysis estimates the GSD from an image of sediment in one of two ways: (i) the so-called geometrical methods (cf. Buscombe *et al.*, 2010), which measure the apparent grain axes of each individual grain using image segmentation techniques (Sime & Ferguson, 2003; Graham *et al.*, 2005, 2010; Chang & Chung, 2012); and (ii) statistical methods, which measure the GSD based on spatial autocorrelation (Rubin, 2004; Barnard *et al.*, 2007; Buscombe, 2008; Buscombe & Masselink, 2009; Warrick *et al.*, 2009; Gallagher *et al.*, 2011; Cheng & Liu, 2015) or spectra of image intensity (Buscombe *et al.*, 2010; Buscombe & Rubin, 2012). However, each of these forms of image analysis has limitations. Geometrical methods, based on edge

detection and segmentation of individual grains, often have difficulty resolving overlapping grains, or touching grains of similar colour or shade, which can lead to oversegmentation and undersegmentation of grains and, thus, has so far made a universally applicable edge detection algorithm elusive (see review by Buscombe, 2013). Conversely, some statistical methods have relied on the time-consuming generation of a site-specific reference image catalogue prior to analysis (Rubin, 2004; Barnard *et al.*, 2007; Buscombe, 2008; Buscombe & Masselink, 2009; Warrick *et al.*, 2009; Gallagher *et al.*, 2011; Di Maria *et al.*, 2016) or otherwise only provide the mean and/or sorting coefficient rather than the full GSD (Buscombe *et al.*, 2010; Buscombe & Rubin, 2012). Buscombe (2013) proposed a statistical method based on wavelet analysis that estimates the full GSD, without the need to isolate and segment each grain and without the need for site-specific calibration. To the authors' knowledge, this method has been tested only on siliciclastic sediment (Buscombe *et al.*, 2014; King *et al.*, 2016).

Sieving and laser diffraction methods assume that particles are spherical and of uniform density (McCave & Syvitski, 1991). Although either or both of these assumptions may often be valid in siliciclastic environments, they are both almost always violated in bioclastic environments (for example, coral reefs), where sediment is largely derived from calcifying organisms (corals, coralline algae, foraminifera, molluscs, etc.) with variable shapes (rods, discs and plates) and densities (Maiklem, 1968; Braithwaite, 1973). Previous methodological comparisons using siliciclastic sediment have shown that sieve and settling tube analysis produce nearly identical GSDs when deposits are well-sorted (Komar & Cui, 1984); sieve and laser diffraction analysis yield similar GSDs for sand-sized material (Cheetham *et al.*, 2008; Di Stefano *et al.*, 2010); and image

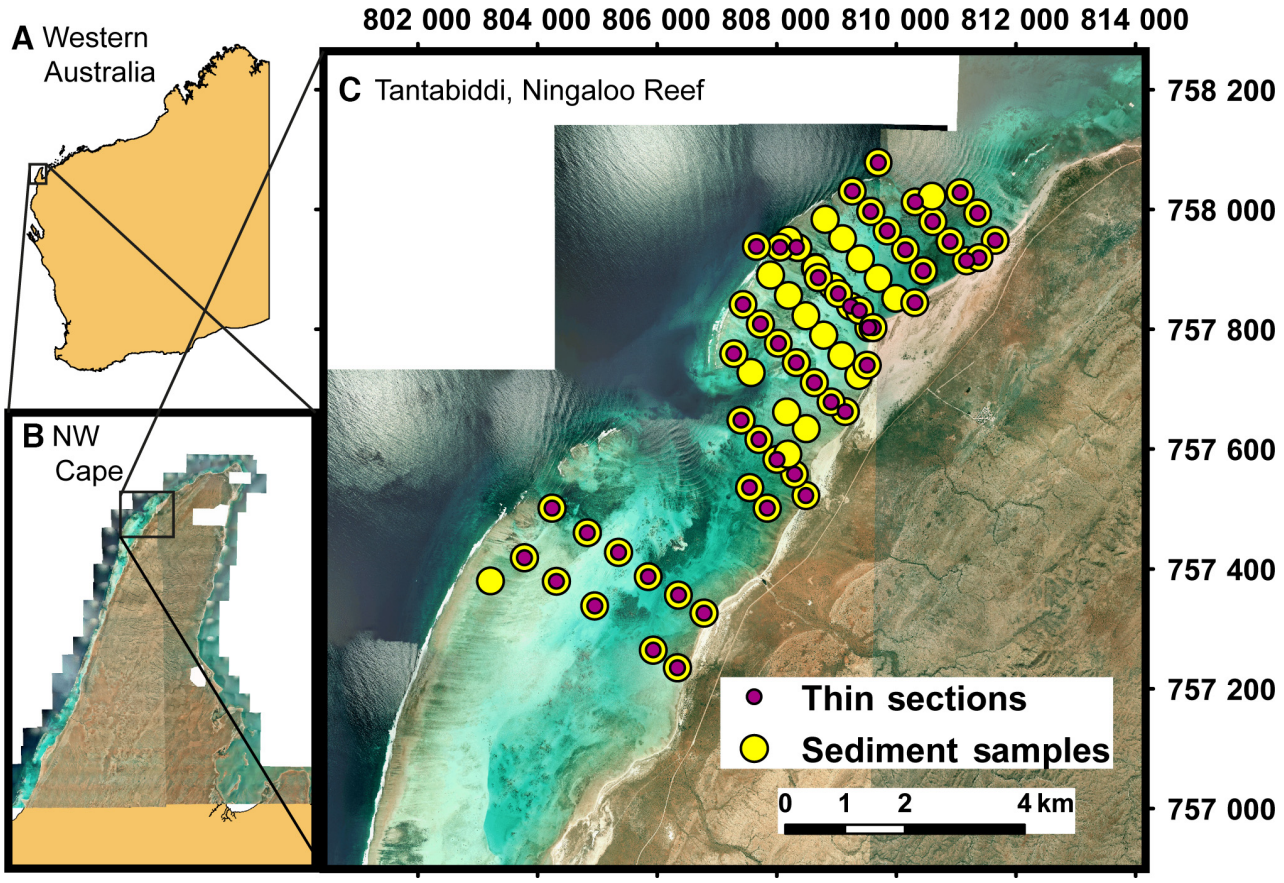

Fig. 1. Map of (A) Western Australia, (B) the north-west (NW) cape of Western Australia and (C) the study site at Tantabiddi, Ningaloo Reef, Western Australia. Aerial imagery is from the SLIP Portal by the Western Australian Land Information System (WALIS) and Landgate (https://www2.landgate.wa.gov.au/). White areas in (C) are due to lack of coverage in the aerial imagery.

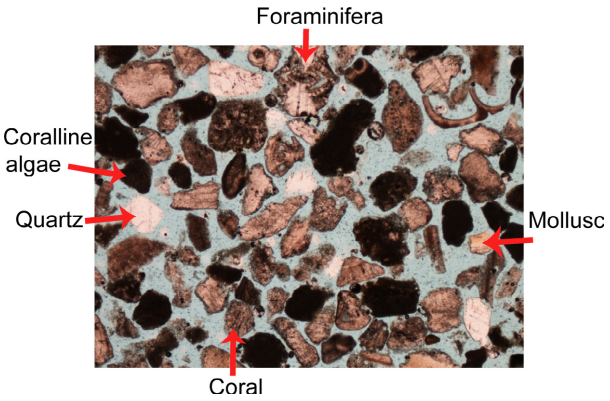

Fig. 2. Example thin-section image used in constituent assemblage analysis. Coral, coralline algae, quartz, mollusc and foraminifera fragments are highlighted.

analysis can produce GSDs within 4% of those measured by sieve and settling tube (Barnard *et al.*, 2007; Gallagher *et al.*, 2011; Buscombe *et al.*, 2014). However, comparative studies in bioclastic environments have suggested that sieve can yield significantly larger mean grain-size estimates (up to 300%) than settling tube for coarse samples (mean >1 mm), smaller mean grain-size estimates in fine samples (mean <1 mm; Kench & McLean, 1997), and that the relationship between sieve and settling tube can be significantly non-linear (Smith & Cheung, 2002). These differences can cause misinterpretations of transport pathways and deposit-forming processes in bioclastic environments (Kench & McLean, 1996; Kench & McLean, 1997).

There remains a gap in the sedimentological literature concerning how results from more modern methods (such as laser diffraction and image analysis) relate to more classic grain-size methods (sieve and settling tube) for bioclastic sediments. This comparison is particularly important given that the more modern methods are usually less time-consuming, achieve greater detail and more accurate analysis of finer material and, for image analysis, can be conducted *in situ*, obviating the need for sample collection and storage, both of which facilitate higher rates of spatial and temporal sampling (Barnard *et al.*, 2007; Gallagher *et al.*, 2011; Buscombe *et al.*, 2014), and hence may yield greater insight into sediment dynamics. Furthermore, it is poorly understood how common settling velocity models, developed from experiments on siliciclastic particles, perform for more irregular, bioclastic sediment. Here, these gaps are addressed by: (i) measuring the GSDs of bioclastic sediment from a nearshore reef environment on the north-west coast of Australia using three common methods (sieve, laser diffraction and image analysis); (ii) calculating settling velocities from the resulting GSDs according to three different models as developed by Gibbs *et al.* (1971), Dietrich (1982) and Ferguson & Church (2004); and (iii) comparing these results against direct measurements of settling velocities. This study will further current understanding of sediment dynamics in bioclastic environments by allowing for conversion of previously existing grain-size distributions to settling velocities and thus allowing for the hydrodynamic properties and transport modes of grains to be established.

METHODS

Study area

'Natural' (n = 73) and 'standard' (n = 2) sediment samples were used in this analysis. The 73 natural samples were collected from Tantabiddi, Ningaloo Reef, Western Australia (21·8714°S, 113·9903°E; Fig. 1). Approximately 500 g of sediment was collected from the top 5 to 7 cm of the seabed at each site. The standard samples were well-rounded, quartz-based sand (D_{50} *ca* 0·3 mm) and CaribSea Aragamax™, an oolitic aragonite sand (D_{50} *ca* 0·5 mm).

This study focused on the sand fraction (0·063 to 2·00 mm) only. Therefore, all samples were washed over a 63 μm sieve and dried to remove silt and clay-sized grains (≤1%); a riffle splitter was then used to generate five statistically equivalent sub-samples. Each of the four grain-size methods (sieve, settling tube, laser diffraction and image analysis) was used on one of the sub-samples to determine the GSD, and the last sub-sample was used to determine the composition of each sample.

Sub-samples for compositional analysis were embedded in epoxy and thin-sectioned (Fig. 2); composition was then determined by identifying a minimum of 300 grains using a petrographic microscope. Grains were divided into eight categories: coral, coralline algae, foraminifera, mollusc, echinoderm, quartz, framework and other.

Grain-size distributions were determined using the modified geometric method of Folk & Ward for sieve, laser diffraction and image analysis (Folk & Ward, 1957; Blott & Pye, 2001); median grain size (D_{50}) was then converted to settling velocity for comparison with measured

settling velocities. Root-mean-square error and mean absolute error were normalized by the range of measured values to give normalized root-mean-square error (NRMSE) and normalized mean absolute error (NMAE); these were then used to compare between results for all the various methods:

$$\mathrm{NRMSE}(\%) = \frac{\sqrt{\frac{\sum\left[\left(\mathrm{Measured}-\mathrm{Estimated}\right)^2\right]}{n}}}{\mathrm{Measured}_{\max} - \mathrm{Measured}_{\min}} * 100 \quad (1)$$

$$\mathrm{NMAE}(\%) = \frac{\frac{1}{n}\sum\left(|\mathrm{Measured} - \mathrm{Estimated}|\right)}{\mathrm{Measured}_{\max} - \mathrm{Measured}_{\min}} * 100 \quad (2)$$

Sediment density measurements

There exists a wide range of sediment density values in the carbonate sediment literature, which is primarily due to the type of density measured (Table 1). Whereas each type of density reported in Table 1 has a specific application (see *Discussion*), for sediment transport applications and settling velocity calculations it is appropriate to use the 'particle density' (ρ_{part}), which corresponds to the specific gravity of a particle (Gibbs *et al.*, 1971; Komar, 1981; Ferguson & Church, 2004) when all intragranular pore spaces of the particle are filled with water (Smith & Cheung, 2003). To directly measure ρ_{part}, a method similar to that used by the American Society for Testing and Materials was employed here for measuring specific gravity (ASTM International, 2010).

Approximately 50 g of sediment was combined with fresh water at a known temperature in a 100 ml volumetric flask and then the solution was sonicated for 1 h (as opposed to boiled) to remove entrapped air. Particle density was then calculated as:

Table 1. Summary of sediment density values found in the literature (*range includes measurements on specific sediment constituents).

Author	Sediment density (g cm^{-3})	Sediment composition	Type of density measured
Berthois & Calvez (1960)	1·16	Foraminifera	Effective density
Jell *et al.* (1965)	1·60 to 2·90*	Foraminifera, coral, green/red calcareous algae	Particle density
Berger & Piper (1972)	1·50	Planktonic foraminifera	Effective density
Neumann & Land (1975)	1·15	Calcareous algae and 'lime mud'	Bulk density
Land (1979)	1·35	Calcareous ooze, *Halimeda*-rich mud, foraminifera-rich sand	Bulk density
Fok-pun & Komar (1983)	1·48	Foraminifera	Effective density
Sadd (1984)	1·50	Coral, molluscs, foraminifera, echinoids, coralline algae	Bulk density
Hubbard *et al.* (1990)	1·20	Coral, molluscs, foraminifera, echinoids, coralline algae	Bulk density
Kench & McLean (1997)	1·85	Coral, coralline algae, alcyonarian spicules, crustaceans, echinoids, *Halimeda*, foraminifera, molluscs	Particle density
Michels (2000)	1·73	Foraminifera	Effective density
Paphitis *et al.* (2002)	2·72 to 2·80*	Mollusc shells	Particle density
Smith & Cheung (2003)	2·59 to 2·78	Foraminifera, coralline algae, molluscs, corals, echinoids, *Halimeda*	Particle density
Harney & Fletcher (2003)	0·70 to 1·56*	Coral, coralline algae, *Halimeda*, foraminifera, molluscs	Bulk density
Morgan & Kench (2014)	1·85	Coral, coralline algae, *Halimeda*, molluscs	Particle density
This study	2·51 to 2·76	Coral, coralline algae, molluscs, foraminifera	Particle density

$$\rho_{\text{part}} = \frac{M_s T}{M_s + M_{\text{FW}} - M_{\text{FSW}}} * \rho_{\text{water}} \qquad (3)$$

where M_s is the mass of dry sand, T is a correction factor based on the temperature of water, M_{FW} is the mass of the volumetric flask filled with water, M_{FSW} is the mass of the volumetric flask with both sand and water, and ρ_{water} is the standard density of fresh water at 20°C (i.e. 1 g cm^{-3}).

The value of ρ_{part} was measured for 20 natural (bulk) sediment samples spanning the range of sub-reef sampling sites; these 20 values were then averaged to calculate a representative ρ_{part} for all natural samples. Similarly, ρ_{part} was measured and then averaged for two sub-samples of each standard (the quartz sand and the aragonite sand). Because there exists a range of sediment density values reported in the literature, even for the same types of measured densities (Table 1), it is necessary to understand the contribution to error in the calculated w_s due to specification of sediment density. Therefore, settling velocities were calculated not only using the measured ρ_{part} values, but also using 1·2 g cm^{-3} (at the lower end of densities reported for carbonate sands) and 1·85 g cm^{-3} (a mid-range density).

Sieve

Approximately 70 g of sediment was analysed through a sieve stack ranging from 4·0 phi (0·063 mm) to −1·0 phi (2 mm) at 0·5 phi intervals (i.e. 11 sieve fractions). Samples were sieved in a mechanical sieve shaker for 15 min, which was sufficient time to allow complete separation into size classes (Román-Sierra *et al.*, 2013). Sediment trapped on each sieve screen was collected and weighed to calculate the GSD.

Settling tube

Settling tube analysis was conducted in a 24 cm diameter, 212 cm tall water column. Between 15 g and 20 g of sediment were wetted to a sample plate and attached to a magnetic holder above the water column. An external trigger was used to simultaneously lower the plate into the water, thus releasing the sediment and starting the timer. Each run lasted 10 min, which was sufficient time to measure the fall velocities of the finest material of interest (*ca* 0·063 mm), with the cumulative mass recorded at 1 Hz. The balance used was accurate to ±0·05 g (±1 SD); which corresponds to *ca* ±0·02 cm sec^{-1} for measured w_s.

Laser diffraction

A Malvern Mastersizer 2000 (Malvern Instruments Limited, Malvern, United Kingdom) was used for laser diffraction (LD) analysis (Cheetham *et al.*, 2008; Di Stefano *et al.*, 2010). Prior to analysis, samples were sieved through a 0 phi (1 mm) sieve, then added to a solution of 10 ml of alkaline sodium hexametaphosphate and 800 ml of deionized water and then ultrasonically stirred for 30 sec (Di Stefano *et al.*, 2010). Because sample preparation removed material >1 mm, only samples that had no fractions coarser than 1 mm from sieve analysis were used for comparison. Laser diffraction converts optical scatter to a GSD using a specified optical model; however, selection of a particular optical model has been shown to have negligible effects on results for sand-sized particles (Blott & Pye, 2006). Therefore, GSDs were calculated using Mie theory and the refractive index of either aragonite (i.e. 1·53 for the natural and aragonite sands) or quartz (i.e. 1·46 for the quartz sand).

Image analysis

Images of sediment samples were collected using a Canon EOS 5D Mark II (Canon Inc., Tokyo, Japan) fitted with a 65 mm macro lens. Sediment samples were arranged on a fixed stage and manually flattened, meaning that the image plane was parallel to the object plane and, therefore, spatial resolution was uniform over the entire image and a single conversion factor (0·0062 mm per pixel) could be used to convert GSD results from pixels to millimetres (Barnard *et al.*, 2007; Gallagher *et al.*, 2011; Buscombe, 2013). Previous tests of image analysis have shown that errors are reduced if multiple images are taken and then averaged; therefore, in this study a total of 20 images were taken for each sample (Barnard *et al.*, 2007; Gallagher *et al.*, 2011; Buscombe, 2013).

A MATLAB® program implementing the algorithm of Buscombe (2013), 'Digital Grain Size', was used to process the images. The method of Buscombe (2013) approximates the GSD using the global power spectral density function derived using a Morlet wavelet. When using digital grain size, there are various options for image processing; the first option is the region of interest (ROI) used to calculate the GSD. The user is allowed to specify the entire image as the ROI or to use a subsection, or multiple subsections of the image as ROIs. To determine which was most

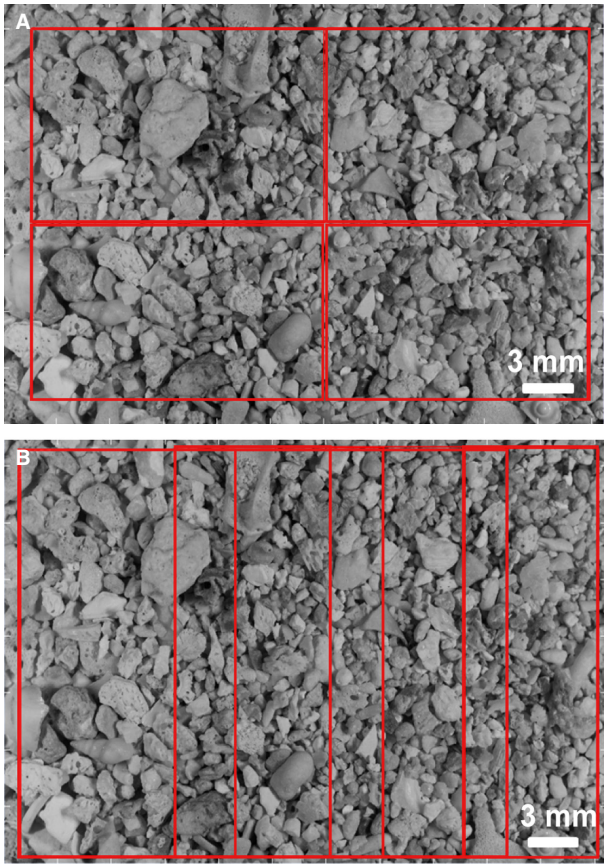

Fig. 3. Examples of (A) non-overlapping regions of interest (ROI) and (B) overlapping ROIs (*ca* 30% overlap) used when calculating grain-size distributions with the digital grain-size graphical user interface (DGS GUI) from Buscombe (2013).

appropriate, a series of tests was performed using the whole image as the ROI, multiple non-overlapping equal-area ROIs, and multiple overlapping equal-area ROIs (Fig. 3).

Other options in DGS include 'flattening' the image, which is a Savitsky–Golay high-pass filter (Savitzky & Golay, 1964) and can help to eliminate errors that are introduced by non-uniform lighting conditions, lens curvature, or the sediment surface being non-parallel to the image plane. These optical artefacts are picked up by spectral analysis as spuriously high variance at wavelengths greater than any grain length scale, which can lead to overestimates of grain size. In order to test the potential effects of this, the algorithm was run with and without flattening the image. To ensure that the algorithm was producing realistic results, a manual 'point count' was conducted on 10 samples following the method of Barnard *et al.* (2007) and compared to the DGS results, which has become a standard way to evaluate the image-derived grain-size estimates with a completely equivalent metric (Warrick *et al.*, 2009; Buscombe *et al.*, 2010, 2014; Buscombe & Rubin, 2012; Buscombe, 2013).

The results of DGS are an 'area by size' measure of grain diameter, whereas sieve, laser diffraction and settling tube are a 'volume by size' or 'mass by size' measure. Although these two measures of grain diameter are not directly comparable, there exists a common method to convert from areal-based to volume-based measures of grain size (Diplas & Sutherland, 1988; Graham *et al.*, 2005, 2012):

$$p(V-W)_i = \frac{p(S)_i * D_i^x}{\sum p(S)_i * D_i^x} \quad (4)$$

where $p(V–W)_i$ is the 'volume by weight' proportion of the ith size fraction, $p(S)_i$ is the image-derived areal proportion of the ith size fraction, D_i is the grain size of the ith size fraction and x is a conversion constant. Diplas & Sutherland (1988) suggest that x should vary between 0 and −1 depending upon porosity (with $x = -1$ when porosity = 0%). According to Diplas & Fripp (1992), it is necessary to use different values for exponent x depending on grain size, but a pragmatic approach is to use an average value for x, which is determined empirically (Diplas *et al.*, 2008). The data from Diplas & Sutherland (1988) suggests $x = -0{\cdot}47$ for natural sediments with *ca* 33% porosity; therefore, when converting to 'volume by size' proportions, both $x = -0{\cdot}5$ and $x = -1{\cdot}0$ were tested here.

Conversion to settling velocity

The equations from Gibbs *et al.* (1971), Dietrich (1982) and Ferguson & Church (2004) were used to convert grain-size results to settling velocities. Gibbs *et al.* (1971) (hereafter 'Gibbs') only accounts for particle size and ρ_{part}:

$$w_s = \frac{-3\mu + \sqrt{9\mu^2 + gr^2\rho(\rho_{part} - \rho)(0{\cdot}015476 + 0{\cdot}19841r)}}{\rho(0{\cdot}011607 + 0{\cdot}14881r)} \quad (5)$$

where μ is kinematic viscosity of water, g is gravitational acceleration, r is grain radius and ρ is fluid density; therefore, measured ρ_{part} and D_{50} values were used for sieve, laser diffraction and image analysis.

Dietrich (1982) (hereafter 'Dietrich') requires ρ_{part}, the Corey (1949) shape factor and the Powers (1953) roundness index (PRI) to determine settling velocity:

$$w_s = R_3 10^{R_1+R_2} \quad (6)$$

where R_1, R_2 and R_3 are fitted equations correcting for particle density, shape and roundness, respectively (see Appendix for equations). While the measured ρ_{part} and the suggested PRI for natural particles (i.e. 3·5) were used for both the standard and natural samples, 0·7 and 0·55 were used for CSF for the standard and natural samples, respectively. The Corey (1949) shape factor for the standard samples is the value suggested by Dietrich (i.e. 0·7), whereas 0·55 is the average CSF determined by Smith & Cheung (2003) for reef-derived material. Dietrich is valid only when nominal diameters (D_n) are used for grain size. Therefore, the sieve and image analysis results required conversion to D_n whereas laser diffraction was directly applicable. Smith & Cheung (2002) proposed an empirical equation to convert sieve-derived D_{50} to D_n for carbonate material ($D_n = 1{\cdot}18{*}D_{50}$). Given that image analysis is comparable to sieve diameters after conversion to 'volume by size' diameters (Kellerhals & Bray, 1971; Diplas & Sutherland, 1988), this equation was used to calculate D_n for both sieve and image analysis results.

Finally, the settling velocity equation proposed by Ferguson & Church (2004) (hereafter 'F&C') was evaluated:

$$w_s = \frac{(\rho_{part} - \rho)gD^2}{C_1\upsilon + (0{\cdot}75C_2(\rho_{part} - \rho)gD^3)^{0{\cdot}5}} \quad (7)$$

where D is either sieve or nominal diameter, and C_1 and C_2 are constants determined by particle shape. Ferguson & Church suggest that values of C_1 and C_2 should be 18 and 0·4, respectively, for smooth spheres; 18 and 1, respectively, for natural sands if sieve diameters are used; 20 and 1·1, respectively, for natural sands if D_n is used; and 24 and 1·2, respectively, for very angular grains. Values of C_1 and C_2 were set equal to 20 and 1·1, respectively, and the same grain diameters as those input to Dietrich (i.e. D_n) were used.

RESULTS

Sediment density and compositional analysis

There is some variability in constituent assemblages across sub-reef environments (i.e. reef crest, reef flat and lagoon) at Ningaloo; however, the sands in the study area are predominantly composed of coral fragments, coralline algae and molluscs (Table 2; Cuttler *et al.*, 2015).

Measured ρ_{part} for the natural, bioclastic sediments was 2·58 ± 0·03 g cm^{-3} (mean ± 1 SD) and showed no relationship with median settling velocity (slope = −0·002 ± 0·004, α = 0·05, P = 0·34). Measured ρ_{part} values for the standard quartz and aragonite sands were 2·64 ± 0 g cm^{-3} and 2·71 ± 0·05 g cm^{-3}, respectively. Varying ρ_{part} from 1·2 to 2·6 g cm^{-3} caused a 22 to 28% change in NRMSE for sieve results, an 11 to 12% change in NRMSE for laser diffraction and a 20% change in NRMSE for image analysis (Table 3).

Comparison of methods

Selection of 'Digital Grain Size' region of interest and conversion to volume by size

Estimated GSDs from each analysis consisting of different ROIs were tested against manual point

Table 2. Constituent assemblages for bulk sediment samples from the sub-reef environments at Tantabiddi, Ningaloo Reef.

Constituent	Reef crest (%)	Reef flat (%)	Lagoon (%)	Channel (%)	Beach (%)
Coral	37	38	36	27	33
Coralline algae	21	19	16	17	14
Mollusc	22	20	19	21	24
Foraminifera	8	7	7	5	6
Echinoderm	1	1	1	0	1
Framework	5	3	4	2	4
Quartz	5	5	16	28	18
Other	1	1	1	1	1

Table 3. Normalized mean absolute error (NMAE) and normalized root-mean-square error (NRMSE) for (A) sieve, (B) laser diffraction and (C) image analysis due to varying sediment density for each settling velocity equation.

	Sediment density					
	1·20 g cm^{-3}		1·85 g cm^{-3}		2·58 g cm^{-3}	
Settling velocity equation	NMAE (%)	NRMSE (%)	NMAE (%)	NRMSE (%)	NMAE (%)	NRMSE (%)
(A) *Sieve*						
Gibbs *et al.* (1971)	33	35	17	18	9	11
Dietrich (1982)	34	37	20	21	8	10
Ferguson & Church (2004)	33	36	17	19	6	8
(B) *Laser diffraction*						
Gibbs *et al.* (1971)	8	14	1	2	6	10
Dietrich (1982)	9	16	3	6	2	4
Ferguson & Church (2004)	9	16	3	5	3	6
(C) *Image analysis*						
Gibbs *et al.* (1971)	24	28	7	8	22	24
Dietrich (1982)	28	31	8	11	16	18
Ferguson & Church (2004)	26	30	8	10	20	21

count results to determine the most suitable ROI. Normalized root-mean-square error progressively improved as the number of ROIs and amount of overlap increased (Fig. 4). Image flattening, however, caused a slight increase in NRMSE; therefore, overlapping ROIs were used (*ca* 30% overlap) without image flattening because this yielded the lowest NRMSE (13%) when compared to manual point counts.

Results of converting image analysis grain sizes from 'area by size' to 'volume by size' are presented in Fig. 5. When compared to sieve analysis, an equivalent measure of grain size, NRMSE is 28% and 16% when x is set to −0·5 and −1·0, respectively; therefore, −1 was used for x in Eq. 4.

Comparison of settling velocity equations

The results of calculated w_s using the three selected equations versus measured w_s using the settling tube are shown in Fig. 6. Settling velocities calculated from image analysis (Fig. 6C) have the highest NMAE and NRMSE, with a maximum of 22% and 24%, respectively. The NMAE and NRMSE from laser diffraction varied from 2 to 6% and 4 to 10%, respectively, for Gibbs, Dietrich and F&C (Fig. 6B), whereas NMAE and NRMSE from sieve diameters varied from 6 to 9% and 8 to 11%, respectively, for Gibbs, Dietrich and F&C (Fig. 6A).

Although Gibbs predicts w_s with comparable NRMSE to Dietrich and F&C, there is a clear trend of increasing overprediction of w_s with increasing observed w_s for sieve and laser diffraction (Fig. 6A and B). Furthermore, whereas the relationships between observed and estimated w_s for sieve and laser diffraction are linear (Fig. 6A and B), the same relationships for image analysis (Fig. 6C) are non-linear, showing maximum discrepancy at mid-range w_s. These trends are consistent for all tested values of ρ_{part}; however, the variability in NRMSE between settling velocity models for measured ρ_{part} (3 to 6%) is much smaller than the range in NRMSE caused by varying ρ_{part} for a given grain-size method and settling velocity model (Table 3).

DISCUSSION

The size and shape of the region of interest (ROI) used in the image analyses influenced the calculated grain-size distribution (GSD; Figs 3 and 4). In general, larger ROIs led to the overestimation of grain size. This response is consistent with Buscombe & Rubin (2012), which showed that image intensity in an image of sediment is a non-stationary random field; therefore, by changing the size and location of the window (i.e. ROI), the second-order (spatial) statistics of image intensity change. Sayles & Thomas (1978) showed that, in such a situation, the variance in the power spectral density is directly proportional to the bandwidth (in the frequency domain) which is related to the window size (in

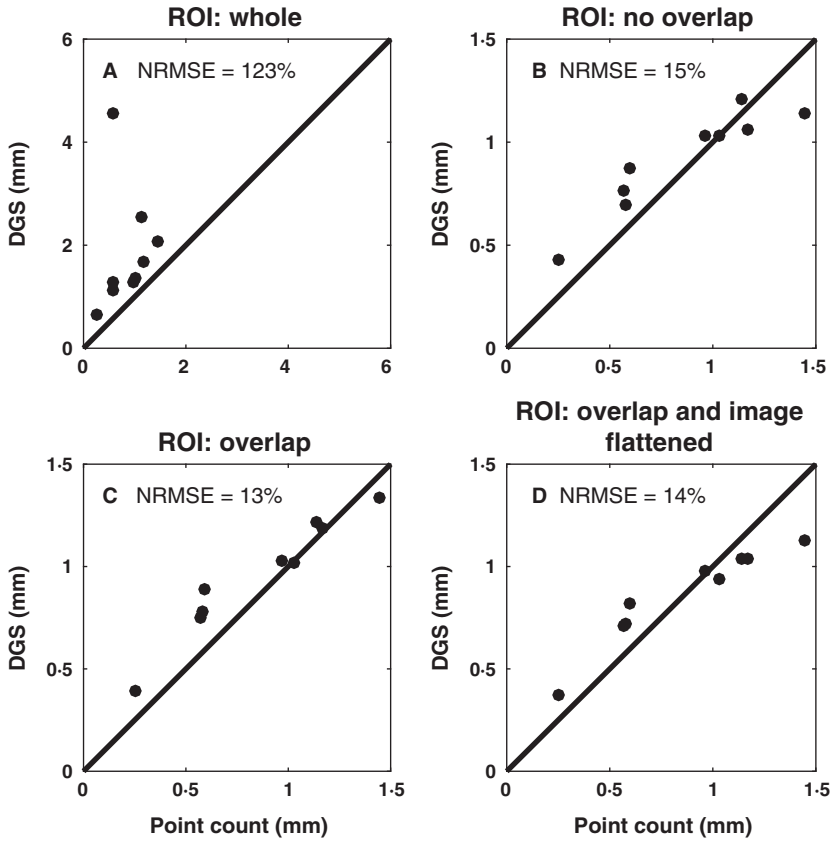

Fig. 4. Comparison of digital grain-size (DGS) algorithm from Buscombe (2013) with manual point count results for D_{50} when the region of interest (ROI) is set to (A) the whole image; (B) multiple, non-overlapping regions; (C) multiple, overlapping regions; and (D) multiple overlapping regions with image flattening.

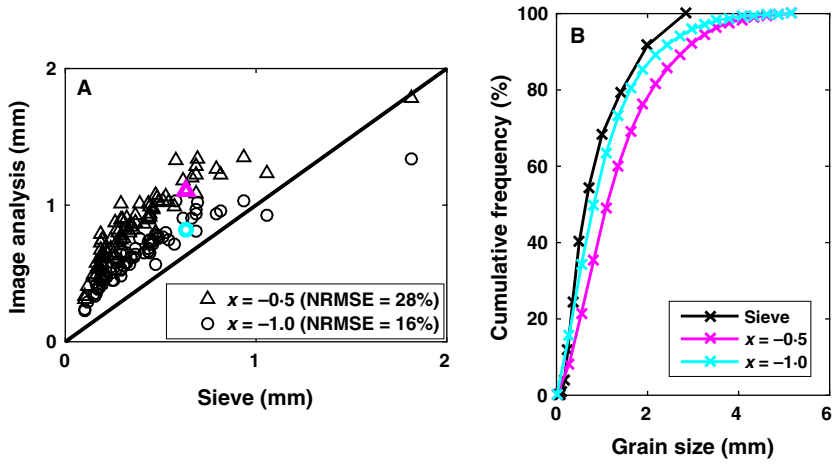

Fig. 5. (A) Comparison of volume by size image analysis D_{50} with sieve D_{50}; squares and circles denote −0·5 and −1·0, respectively, for the value of x in Eq. 4. (B) Cumulative frequency curves for sieve, $x = -0{\cdot}5$, and $x = -1{\cdot}0$ for the sample highlighted in (A).

the spatial domain). In this case, the effect was to coarse-bias the estimates of grain size for large ROIs. Given that the effects of ROI size on grain-size estimates are likely to be different for each sedimentary population, being related to numerous factors, such as the ratio of grain size to window size, grain sorting, orientation and shape, in practice, the size and number of ROIs should ideally be treated as tunable parameters to be determined empirically, such as here, in the practical implementation of the method of Buscombe (2013). It is suggested that averaging results from large numbers of relatively small ROIs should work best in most cases; however, caution should be taken when applying image analysis to intermediate settling velocity material (i.e. medium sand) because this material yielded the highest errors (Fig. 6C).

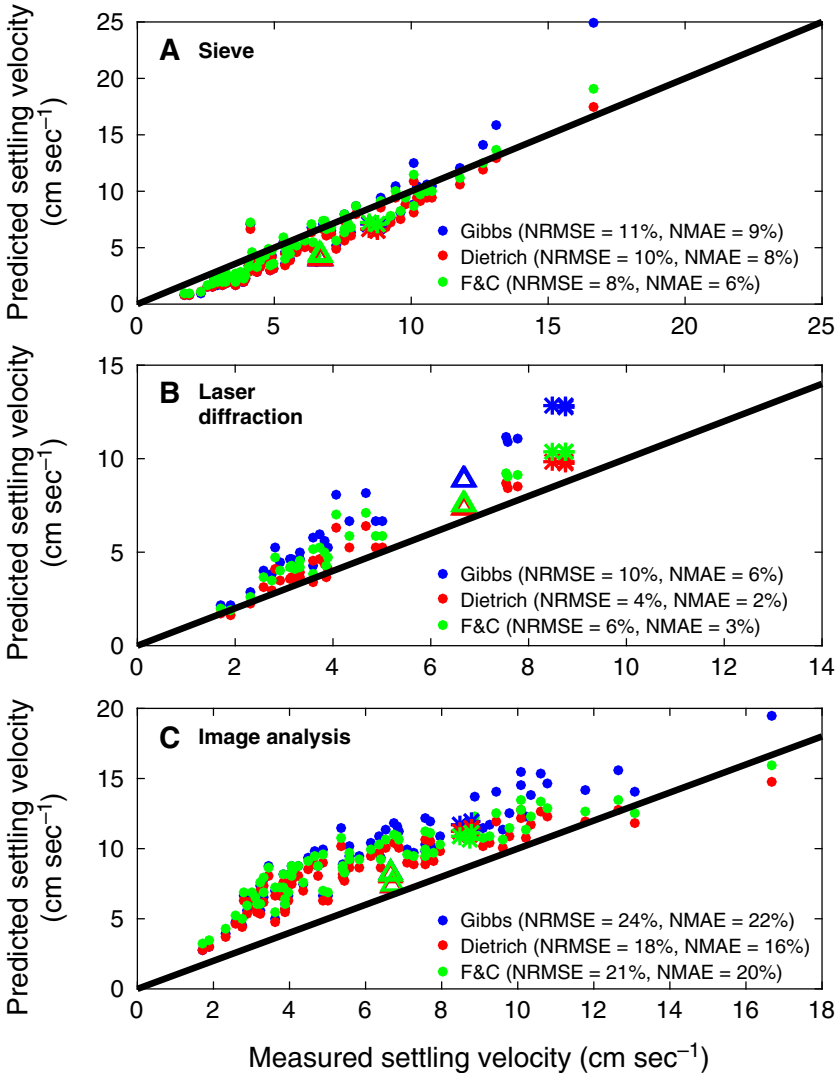

Fig. 6. Comparison of equations used to convert (A) sieve, (B) laser diffraction and (C) image analysis grain sizes to settling velocity. In all panels, blue indicates the Gibbs *et al.* (1971) equation, red indicates Dietrich (1982) and green indicates Ferguson & Church (2004); asterisks indicate aragonite sand standard and triangles indicate quartz sand standard.

Varying sediment density across the range of reported values (1·15 to 2·8 g cm^{-3}; Table 1) caused an 11 to 28% range in NRMSE depending upon settling velocity model and grain-size method (Table 3). This result highlights not only the importance of using an accurate sediment density in settling velocity calculations but also the need to understand why there exists such a range in reported values. This range is a function of how different investigators define the density of their sediments, the nature of their study, the distinct ways carbonate producers calcify and the inherent diversity of sediment constituents within the sediment pool. Studies aimed at the movement of specific facies (for example, foraminifera) often report an 'effective' density for irregularly shaped particles that implicitly assumes a particle of an equivalent spherical diameter whose density matches the observed settling velocity (Berthois & Calvez, 1960; Berger & Piper, 1972; Fok-pun & Komar, 1983). Studies aimed at constructing reef-scale or system-scale budgets of carbonate chemistry, however, often report a 'bulk' sediment density (ρ_{bulk}), which includes the microporosity of the particles (ϕ_{part}) and the mineral density [$\rho_{mineral}$; for example, $\rho_{bulk} = \rho_{mineral} * (1 - \phi_{part})$] so that changes in the mass of calcium carbonate can be computed from changes in sediment volume (Stearn *et al.*, 1977; Land, 1979; Grigg, 1982; Sadd, 1984; Hubbard *et al.*, 1990). Previous examinations of the porosity of specific sediment constituents have shown that corals and coralline algae are *ca* 50 to 60% porous (Stearn *et al.*, 1977; Grigg, 1982); therefore, ρ_{bulk} *ca* 1·5 g cm^{-3} seems to be a reasonable value for budget calculations (see appendix in Sadd, 1984, for example calculations).

Finally, studies aimed at understanding the physical suspension, transport and deposition of sediments generally report the average density of the particles suspended in the fluid (i.e. ρ_{part}) which includes the water that occupies the microporosity of the sediment grains [for example, $\rho_{part} = \rho_{mineral} * (1-\phi_{part}) + \rho * \phi_{part}$] so as to best represent their hydraulic behaviour in a moving fluid (Kench & McLean, 1997; Paphitis *et al.*, 2002; Smith & Cheung, 2003). Both this study and the only other study, to the authors' knowledge, that measured ρ_{part} with a similar method reported a value of *ca* 2·6 g cm^{-3} (Smith & Cheung, 2003); however, other transport studies have used a value of 1·85 g cm^{-3} (Kench & McLean, 1997; Morgan & Kench, 2014), which originates from component-specific measurements by Jell *et al.* (1965). This difference in ρ_{part} can be attributed to a variety of possible factors including: sediment composition, mean grain size, measurement technique and depositional environment. Sediment composition is probably not the cause because all three studies had similar constituent assemblages. Although the sediment samples studied by Kench & McLean (1997) generally had a larger mean grain size, both the results here and those of Smith & Cheung (2003) showed that ρ_{part} was independent of grain size. Unfortunately, Jell *et al.* (1965) did not explain how specific gravity was determined; therefore, it is difficult to evaluate their measurement technique against their derived values. Depositional environment could be an important factor, because the present study and that of Smith & Cheung (2003) both analysed sediments from fringing reefs, whereas Kench & McLean (1997) analysed sediments from an atoll system. If it is assumed that 1·85 g and 2·6 g cm^{-3} are representative values for atoll systems and fringing reefs, respectively, then one explanation for the difference in ρ_{part} could be the age of sediments in the respective systems. For example, sands in Hawaiian fringing reef systems have been shown to be derived from older (hundreds to thousands of years old) material (Harney *et al.*, 2000) and material from the top 1 m of a lagoon core at Tantabiddi has been dated to *ca* 5000 years (Collins *et al.*, 2003). However, work in reef island systems has shown that sediment is derived from modern (tens of years old) sources (for example, modern reef calcifiers; Yamano *et al.*, 2000; Dawson *et al.*, 2012). It is therefore possible that due to their age, fringing reef sediments no longer retain their original internal porosities (for example, taphonomic processes and/or internal microboring could alter internal structures) and therefore have a higher ρ_{part}; reef island sands, on the other hand, probably still retain the microstructure of the biogenic source material and therefore could have a lower ρ_{part}. However, because there have been so few actual measurements of ρ_{part} in various bioclastic environments, there is a clear need for more work like the present contribution to resolve these questions and to understand the range of sediment densities applicable to these different systems.

Shape is also a key factor when determining settling velocities, as any divergence from spherical can only lead to decreases in settling velocity when compared with spherical particles of an equivalent weight (Dietrich, 1982). Although the Dietrich and Ferguson & Church models explicitly account for particle shape, the Gibbs equation does not. Shape effects are visible in the Gibbs data for sieve and laser diffraction as increasing overestimation of settling velocity with increasing measured settling velocity (Fig. 6A and B). Similar results have been shown in previous comparisons between sieve and laser diffraction measurements (Konert & Vandenberghe, 1997; Blott & Pye, 2006), as well as sieve and settling tube measurements (Komar & Cui, 1984; Kench & McLean, 1997). Shape effects on settling velocity are primarily due to the fact that natural particles settle perpendicular to their largest projected area, which increases drag on the particle and leads to a slower settling velocity (Dietrich, 1982; Komar & Cui, 1984). This shape effect has been shown to reduce settling velocities by a maximum of *ca* 2× for particles coarser than *ca* 1·4 mm, or by *ca* 1·5× for those smaller than *ca* 1·4 mm (Dietrich, 1982).

In bioclastic environments, shape is inherently linked to the specific organism from which the particle is derived (Perry *et al.*, 2011); therefore, the constituent assemblage could explain some of the increasing discrepancy between measured and estimated settling velocities for faster settling samples. Past studies of carbonate sediment settling have shown that typical constituents have specific settling behaviours that enhance the disagreement between sieve and settling tube results (Maiklem, 1968; Braithwaite, 1973; Smith & Cheung, 2003). Mollusc shells, for example, have large physical sizes but tend to settle with a spiral motion; this settling style will lead to slow settling velocities, whereas their shape will cause them to be

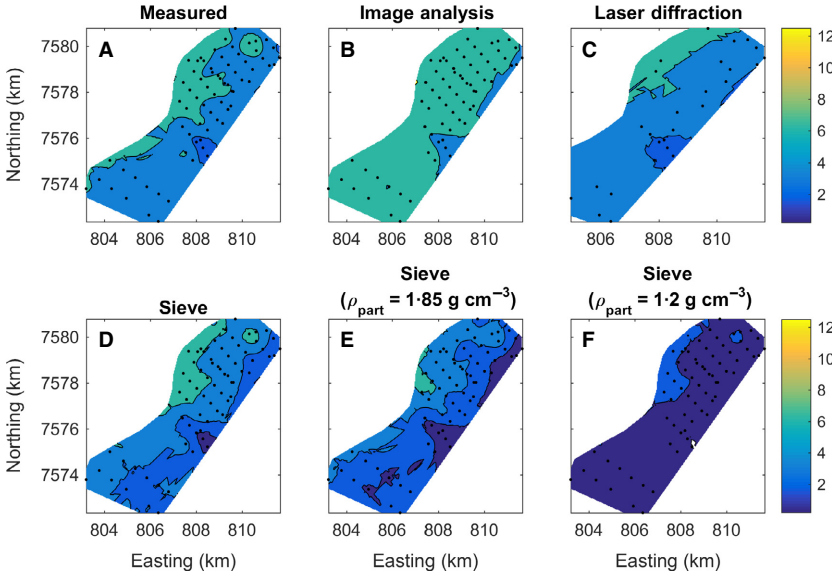

Fig. 7. Spatial maps depicting settling velocity boundaries at Tantabiddi, Ningaloo Reef, for (A) measured settling velocities, (B) image analysis-derived settling velocities, (C) laser diffraction-derived settling velocities and (D) sieve-derived settling velocities. For (B), (C) and (D), the Dietrich equation was used with PRI = 3·5, CSF = 0·55 or 0·7 and ρ_{part} = measured values; (E) and (F) depict the settling velocity boundaries for sieve-derived measurements when ρ_{part} = 1·85 or 1·2 g cm^{-3}, respectively.

trapped on coarser sieves (Maiklem, 1968; Braithwaite, 1973; Smith & Cheung, 2003). Indeed, the thin-section analysis showed an increasing percentage of mollusc fragments (both broken and intact) in faster settling deposits collected from Ningaloo which, based on their settling behaviour and irregular shape, could help to explain the overestimation of calculated w_s by Gibbs for these samples.

When shape was accounted for by the settling velocity model (i.e. Dietrich or F&C), NRMSE was reduced by up to 6% (Table 3) and the velocity-dependent bias was removed from sieve and laser diffraction results (Fig. 6A and B).

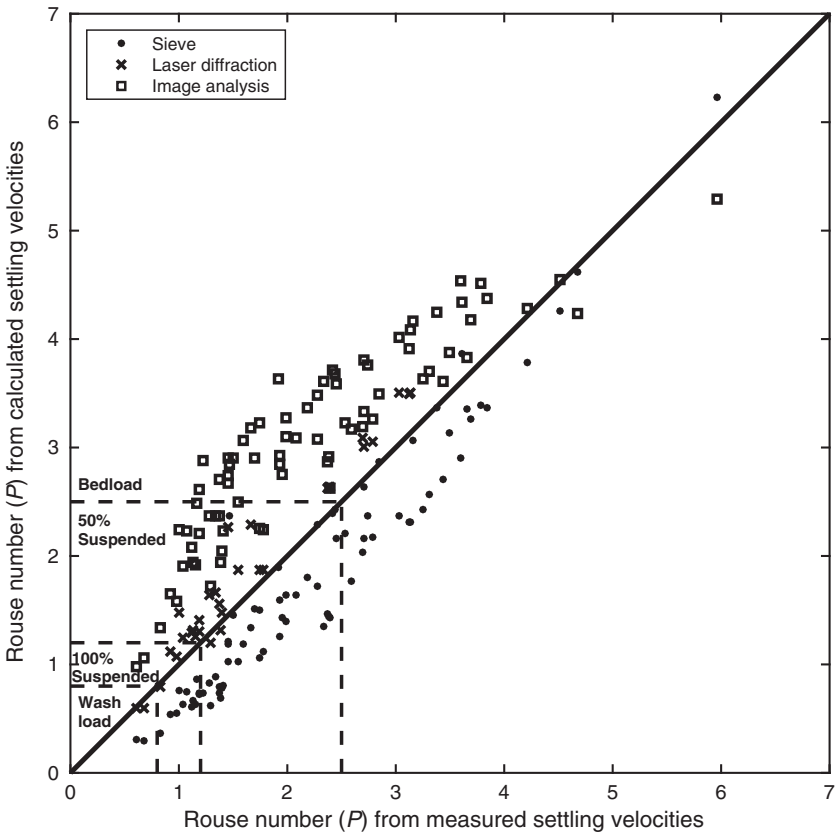

Fig. 8. Comparison of the Rouse number (P) from measured and calculated settling velocities. Values are shown for results from sieve, laser diffraction and image analysis.

Furthermore, although F&C performs better for sieve, Dietrich is more accurate for laser diffraction and image analysis and is also a more thorough treatment of particle irregularities. Therefore, Dietrich is suggested here as the preferred equation for settling velocity calculations.

In practical applications to bioclastic environments, settling velocities can be used to delineate various sub-environment zones (i.e. different reef zones) and to predict sediment transport mode; both of these applications are critical to understanding and predicting sediment transport pathways through these systems. Kench (1997) suggested that bioclastic sediment can be grouped into distinct settling velocity fractions, ranging from very slow settling (0·4 to 0·8 cm sec^{-1}) to very fast settling (25 cm sec^{-1} to 50 cm sec^{-1}). Using this classification and measured settling velocities, there are clearly three settling velocity zones at Tantabiddi (Fig. 7A): (i) fast–moderate settling on the fore reef/reef crest (6·3 cm sec^{-1} to 12·5 cm sec^{-1}); (ii) moderate settling on the reef flat and majority of the lagoon (3·1 cm sec^{-1} to 6·3 cm sec^{-1}); and (iii) moderate–slow settling in the nearshore area of the southern channel (1·6 cm sec^{-1} to 3·1 cm sec^{-1}).

Although no method is able to perfectly match the measured spatial variation, laser diffraction reproduces the correct number and location zones (Fig. 7C); sieve reproduces the correct spatial pattern, but it under-predicts the slowest settling material (Fig. 7D); and, finally, when image analysis is used, there is no indication of the slowest settling zone and the fastest settling zone occupies a much larger area than measured. Furthermore, similar results are observed when ρ_{part} is varied for sieve results (i.e. variable number of zones and under-prediction of settling velocity) (Fig. 7E and F).

Settling velocity can also be used to determine entrainment and transport mode (bedload, suspended load, or wash load) in aquatic environments, most commonly in the context of the Rouse number, $P = w_s/ku_*$, where k is the von Karman constant (0·4) and u_* is the shear velocity (Rouse, 1937). Sand ripples have been observed in the Ningaloo lagoon (*ca* 10 cm amplitude and *ca* 50 cm wavelength) and wave-induced ripple migration (i.e. bedload transport) has been suggested to be the primary mode of sediment supply to the shoreline (Cuttler *et al.*, 2015).

Using Dietrich-derived settling velocities and a typical wave-induced u_* value of 7 cm sec^{-1} (Cuttler *et al.*, 2015) to calculate P for the lagoon samples, the use of laser diffraction and image analysis overestimates P (i.e. trend towards predicting bedload transport), whereas the use of sieve slightly underestimates P (Fig. 8); however, the use of each grain-size method would suggest that the majority of lagoon deposits are mobilized as bedload or partial suspended load under normal wave conditions (significant wave height *ca* 1 to 2 m), thus supporting the hypothesis that ripple migration is crucial to shoreline maintenance at Ningaloo.

CONCLUSIONS

Settling velocity is a common characteristic of sedimentary deposits that can be used to understand sediment dynamics in aquatic environments. Although errors in predicted settling velocities can be up to 20%, these errors are still small relative to the natural range of settling velocities of sand-sized material (0·05 to 0·30 cm sec^{-1}, or a variation of *ca* 83%; Smith & Cheung, 2003; Ferguson & Church, 2004). Furthermore, although image analysis had the highest errors, the authors still encourage the use (with caution) and development of this technique because the greater spatial and temporal sampling it provides will greatly outweigh a slight increase in error.

Collectively, the results suggest that any of these common grain-size analysis techniques and settling velocity models, which were originally developed for siliciclastic sediments, can be used to predict settling velocities of irregularly shaped bioclastic sediments with reasonable accuracy; however, this agreement is improved when models account for shape effects. These results particularly highlight the importance of using an accurate measure of sediment density when calculating settling velocity because an incorrect density can cause a change in normalized root-mean-square error (NRMSE) of up to 28%. The present authors suggest the use of the Dietrich (1982) model for estimating settling velocity because it is more accurate for more modern, time-saving techniques and, in general, is a more thorough treatment of particle irregularities. Finally, this analysis will allow for the conversion of grain-size data from a variety of bioclastic environments to be converted to settling velocities for comparison; this will greatly enhance current understanding of sediment dynamics and transport processes in these environments.

ACKNOWLEDGEMENTS

The authors would like to thank Curt Storlazzi, Michael Church and one anonymous reviewer for helpful comments on this manuscript. This project was funded by the Western Australian Marine Institute (WAMSI) Dredging Science Note (Theme 2/3), an Australian Research Council (ARC) Future Fellowship (FT110100201) and ARC Discovery Project grant (DP140102026) to RL. MC is supported by a Scholarship for International Research Fees (SIRF) and a University International Stipend (UIS). Any use of trade, product, or firm names is for descriptive purposes only and does not imply endorsement by the US government. The DGS program of Buscombe (2013) for image-based grain-size analysis is available in Python (https://github.com/dbuscombe-usgs/pyDGS) and Matlab® (https://github.com/dbuscombe-usgs/DGS).

NOMENCLATURE

C_1, C_2	Empirical constants from settling velocity equation of Ferguson & Church (2004)
CSF	Corey (1949) shape factor
D	Grain size (mm)
D_*	Non-dimensional grain size
D_{50}	Median grain size (mm)
D_n	Nominal diameter (mm)
DGS	Digital Grain Size algorithm developed by Buscombe (2013)
g	Gravitational acceleration (m sec^{-2})
GSD	Grain-size distribution
k	Von Karman's constant
M_s	Mass of dry sand (g)
M_{FW}	Mass of volumetric flask with fresh water (g)
M_{FSW} (g)	Mass of volumetric flask with sand and water
n	Sample size
NMAE	Normalized mean absolute error
NRMSE	Normalized root-mean-square error (%)
$p(V–W)_i$	'Volume by weight' proportion of the ith size fraction
$p(S)_i$	Image-derived areal proportion of the ith size fraction
P	Rouse (1937) parameter
PRI	Powers (1953) roundness index
r	Grain radius (cm)
R_1	Empirical equation from Dietrich (1982) relating settling velocity to particle density and size
R_2	Empirical equation from Dietrich (1982) relating settling velocity to particle shape
R_3	Empirical equation from Dietrich (1982) relating settling velocity to particle roundness
ROI	Region of interest used to calculated grain-size distribution with the digital grain-size algorithm of Buscombe (2013)
T	Correction factor determined by temperature of fresh water
u_*	Shear velocity (m sec^{-1})
w_s	Settling velocity (cm sec^{-1})
W_*	Non-dimensional settling velocity
x	Empirical constant for conversion (Eq. 4)
μ	Dynamic viscosity (kg m^{-1} sec^{-1})
v	Kinematic viscosity (m^2 sec^{-1})
ρ	Fluid density (g cm^{-3})
ρ_{bulk}	Bulk density (g cm^{-3})
$\rho_{mineral}$	Mineral density (g cm^{-3})
ρ_{part}	Particle density (g cm^{-3})
ϕ_{part}	Particle porosity

REFERENCES

ASTM International (2010) *Standard Test Methods for Specific Gravity of Soil Solids by Water Pycnometer*. ASTM International, West Conshohocken, PA, doi:10.1520/D0854-10.2.

Barnard, P.L., **Rubin, D.M.**, **Harney, J.** and **Mustain, N.** (2007) Field test comparison of an autocorrelation technique for determining grain size using a digital "beachball" camera versus traditional methods. *Sed. Geol.*, **201**, 180–195.

Berger, H. and **Piper, D.J.W.** (1972) Planktonic foraminifera: differential settling, dissolution and redeposition. *Limnol. Oceanogr.*, **17**, 275–287.

Berthois, L. and **Calvez, L.E.** (1960) Etude de la vitesse de chute des coquilles de foraminifères planctoniques dans un fluide comparativement a celle des grains de quartz. *Revue des Travaux de l'Institut des Pêches Maritimes*, **24**, 293–301.

Birch, G. and **Taylor, S.** (1999) Source of heavy metals in sediments of the Port Jackson estuary, Australia. *Sci. Total Environ.*, **227**, 123–138.

Blott, S.J. and **Pye, K.** (2001) GRADISTAT: a grain size distribution and statistics package for the analysis of unconsolidated sediments. *Earth Surf. Proc. Land.*, **26**, 1237–1248.

Blott, S.J. and **Pye, K.** (2006) Particle size distribution analysis of sand-sized particles by laser diffraction: an experimental investigation of instrument sensitivity

and the effects of particle shape. *Sedimentology*, **53**, 671–685.

Braithwaite, C. (1973) Settling behaviour related to sieve analysis of skeletal sands. *Sedimentology*, **20**, 251–262.

Buscombe, D. (2008) Estimation of grain-size distributions and associated parameters from digital images of sediment. *Sed. Geol.*, **210**, 1–10.

Buscombe, D. (2013) Transferable wavelet method for grain-size distribution from images of sediment surfaces and thin sections, and other natural granular patterns. *Sedimentology*, **60**, 1709–1732.

Buscombe, D. and **Masselink, G.** (2009) Grain-size information from the statistical properties of digital images of sediment. *Sedimentology*, **56**, 421–438.

Buscombe, D. and **Rubin, D.M.** (2012) Advances in the simulation and automated measurement of well-sorted granular material: 1. Simulation. *J. Geophys. Res.*, **117**, F02001.

Buscombe, D., **Rubin, D.M.** and **Warrick, J.A.** (2010) A universal approximation of grain size from images of noncohesive sediment. *J. Geophys. Res.*, **115**, 1–17.

Buscombe, D., **Rubin, D.M.**, **Lacy, J.R.**, **Storlazzi, C.D.**, **Hatcher, G.**, **Chezar, H.**, **Wyland, R.** and **Sherwood, C.R.** (2014) Autonomous bed-sediment imaging-systems for revealing temporal variability of grain size. *Limnol. Oceanogr: Methods*, **12**, 390–406.

Chang, F.-J. and **Chung, C.-H.** (2012) Estimation of riverbed grain-size distribution using image-processing techniques. *J. Hydrol.*, **440–441**, 102–112.

Cheetham, M.D., **Keene, A.F.**, **Bush, R.T.**, **Sullivan, L.A.** and **Erskine, W.D.** (2008) A comparison of grain-size analysis methods for sand-dominated fluvial sediments. *Sedimentology*, **55**, 1905–1913.

Cheng, N.S. (1997) Simplified settling velocity formula for sediment particle. *J. Hydraul. Eng.*, **123**, 149–152.

Cheng, Z. and **Liu, H.** (2015) Digital grain-size analysis based on autocorrelation algorithm. *Sed. Geol.*, **327**, 21–31.

Collins, L.B., **Zhu, Z.R.**, **Wyrwoll, K.H.** and **Eisenhauer, A.** (2003) Late Quaternary structure and development of the northern Ningaloo Reef, Australia. *Sed. Geol.*, **159**, 81–94.

Corey, A.T. (1949) Influence of shape on the fall velocity of sand grains. Colorado A & M College, Fort Collins, unpub. Master's thesis, 102 pp.

Cuttler, M., **Lowe, R.J.**, **Hansen, J.E.**, **Falter, J.L.** and **Pomeroy, A.W.M.** (2015) Grainsize, composition and bedform patterns in a fringing reef system. *Proc. Coastal Sed.*, San Diego, CA.

Dawson, J.L., **Hua, Q.** and **Smithers, S.G.** (2012) Benthic foraminifera : their importance to future reef island resilience. *Proc. 12th Int. Coral Reef Symp.*, Cairns, Australia.

Di Maria, F., **Bianconi, F.**, **Micale, C.**, **Baglioni, S.** and **Marionni, M.** (2016) Quality assessment for recycling aggregates from construction and demolition waste: an image-based approach for particle size estimation. *Waste Manage. (Oxford)*, **48**, 344–352.

Di Stefano, C., **Ferro, V.** and **Mirabile, S.** (2010) Comparison between grain-size analyses using laser diffraction and sedimentation methods. *Biosyst. Eng.*, **106**, 205–215.

Dietrich, W.E. (1982) Settling velocity of natural particles. *Water Resour. Res.*, **18**, 1615–1626.

Diplas, P. and **Fripp, J.B.** (1992) Properties of various sediment sampling procedures. *J. Hydraul. Eng.*, **118**, 955–970.

Diplas, P. and **Sutherland, A.J.** (1988) Sampling techniques for gravel sized sediments. *J. Hydraul. Eng.*, **114**, 484–501.

Diplas, P., **Kuhnle, R.A.**, **Gray, J.R.**, **Glysson, G.D.** and **Edwards, T.E.** (2008) Sediment transport measurements. In: *Sedimentation Engineering: Processes, Measurements, Modeling, and Practice* (Ed. M.H. Garcia), **110**, 307–353. American Society of Civil Engineering Manuals and Reports on Engineering Practice, Reston, VA.

Ferguson, R.I. and **Church, M.** (2004) A simple universal equation for grain settling velocity. *J. Sed. Res.*, **74**, 933–937.

Fok-pun, L. and **Komar, P.D.** (1983) Settling velocities of planktonic foraminifera : density variations and shape effects. *J. Foramin. Res.*, **13**, 60–68.

Folk, R.L. and **Robles, R.** (1964) Carbonate sands of isla perez, alacran reef complex, Yucatan. *J. Geol.*, **72**, 255–292.

Folk, R.L. and **Ward, W.C.** (1957) Brazos River Bar : a study in the significance of grain size parameters. *J. Sed. Petrol.*, **27**, 3–26.

Gallagher, E.L., **MacMahan, J.**, **Reniers, A.J.H.M.**, **Brown, J.** and **Thornton, E.B.** (2011) Grain size variability on a rip-channeled beach. *Mar. Geol.*, **287**, 43–53.

Gibbs, R.J., **Matthews, M.D.** and **Link, D.A.** (1971) The relationship between sphere size and settling velocity. *J. Sed. Res.*, **41**, 7–18.

Graham, D.J., **Rice, S.P.** and **Reid, I.** (2005) A transferable method for the automated grain sizing of river gravels. *Water Resour. Res.*, **41**, W07020.

Graham, D.J., **Rollet, A.J.**, **Piégay, H.** and **Rice, S.P.** (2010) Maximizing the accuracy of image-based surface sediment sampling techniques. *Water Resour. Res.*, **46**, 1–15.

Graham, D., **Rollet, A.J.**, **Rice, S.P.** and **Piégay, H.** (2012) Conversions of surface grain-size samples collected and recorded using different procedures. *J. Hydraul. Eng.*, **138**, 839–849.

Grigg, R.W. (1982) Darwin Point: a threshold for atoll formation. *Coral Reefs*, **1**, 29–34.

Harney, J.N. and **Fletcher, C.H.** (2003) A budget of carbonate framework and sediment production, Kailua Bay, Oahu, Hawaii. *J. Sed. Res.*, **73**, 856–868.

Harney, J.N., **Grossman, E.E.**, **Richmond, B.M.** and **Fletcher, C.H., III** (2000) Age and composition of carbonate shoreface sediments, Kailua Bay, Oahu, Hawaii. *Coral Reefs*, **19**, 141–154.

Hubbard, D.K., **Miller, A.I.** and **Scaturo, D.** (1990) Production and cycling of calcium carbonate in a shelf-edge reef system (St. Croix, U.S. Virgin Islands): applications to the nature of reef systems in the fossil record. *J. Sed. Petrol.*, **60**, 335–360.

Jell, J.S., **Maxwell, W.H.G.** and **McKellar, R.G.** (1965) The significance of the larger foraminifera in the Heron Island Reef Sediments. *J. Paleontol.*, **39**, 273–279.

Kellerhals, P. and **Bray, D.I.** (1971) Sampling procedures for coarse fluvial sediments. *J. Hydraul. Eng.*, **97**, 1165–1180.

Kench, P.S. (1997) Contemporary sedimentation in the Cocos (Keeling) Islands, Indian Ocean: interpretation using settling velocity analysis. *Sed. Geol.*, **114**, 109–130.

Kench, P.S. and **McLean, R.F.** (1996) Hydraulic characteristics of bioclastic deposits: new possibilities for environmental interpretation using settling velocity fractions. *Sedimentology*, **43**, 561–570.

Kench, P.S. and **McLean, R.F.** (1997) A comparison of settling and sieve techniques for the analysis of bioclastic sediments. *Sed. Geol.*, **109**, 111–119.

King, G.E., **Herman, F.**, **Lambert, R.**, **Valla, P.G.** and **Guralnik, B.** (2016) Multi-OSL-thermochronometry of feldspar. *Quart. Geochronol.*, **33**, 76–87.

Komar, P.D. (1981) The applicability of the Gibbs equation for grain settling velocities to conditions other than quartz grains in water. *J. Sed. Petrol.*, **51**, 1125–1132.
Komar, P. and **Clemens, K.** (1986) The relationship between a grain's settling velocity and threshold of motion under unidirectional currents. *J. Sed. Res.*, **56**, 258–266.
Komar, P.D. and **Cui, B.** (1984) The analysis of grain-size measurements by sieving and settling-tube techniques. *J. Sed. Petrol.*, **54**, 603–614.
Konert, M. and **Vandenberghe, J.** (1997) Comparison of laser grain size analysis with pipette and sieve analysis: a solution for the underestimation of the clay fraction. *Sedimentology*, **44**, 523–535.
Land, L.S. (1979) The fate of reef-derived sediment on the north Jamaican island slope. *Mar. Geol.*, **29**, 55–71.
Larcombe, P., **Costen, A.** and **Woolfe, K.J.** (2001) The hydrodynamic and sedimentary setting of nearshore coral reefs, central Great Barrier Reef shelf, Australia: Paluma Shoals, a case study. *Sedimentology*, **48**, 811–835.
Le Roux, J.P. (1992) Settling velocity of spheres: a new approach. *Sed. Geol.*, **81**, 11–16.
Le Roux, J.P. (2002) Shape entropy and settling velocity of natural grains. *J. Sed. Res.*, **72**, 363–366.
Maiklem, W.R. (1968) Some hydraulic properties of bioclastic carbonate grains. *Sedimentology*, **10**, 101–109.
McCave, I.N. and **Syvitski, J.P.M.** (1991) Principles and methods of geological particle size analysis. In: *Principles, Methods, and Application of Particle Size Analysis* (Ed. J.P.M. Syvitski), p. 368. Cambridge University Press, New York.
Michels, K.H. (2000) Inferring maximum geostrophic current velocities in the Norwegian-Greenland Sea from settling-velocity measurements of sediment surface samples: methods, applications and results. *J. Sed. Res.*, **70**, 1036–1050.
Miller, M.C., **McCave, I.N.** and **Komar, P.D.** (1977) Threshold of sediment motion under unidirectional currents. *Sedimentology*, **24**, 507–527.
Morgan, K.M. and **Kench, P.S.** (2014) A detrital sediment budget of a Maldivian reef platform. *Geomorphology*, **222**, 122–131.
Neumann, A.C. and **Land, L.S.** (1975) Lime mud deposition and calcareous algae in the Bight of Abaco, Bahamas: a budget. *J. Sed. Petrol.*, **45**, 763–786.
Paphitis, D., **Collins, M.B.**, **Nash, L.A.** and **Wallbridge, S.** (2002) Settling velocities and entrainment thresholds of biogenic sands (shell fragments) under unidirectional flow. *Sedimentology*, **49**, 211–225.
Perry, C.T., **Kench, P.S.**, **Smithers, S.G.**, **Riegl, B.**, **Yamano, H.** and **O'Leary, M.J.** (2011) Implications of reef ecosystem change for the stability and maintenance of coral reef islands. *Global Change Biol.*, **17**, 3679–3696.
Powers, M.C. (1953) A new roundness scale for sedimentary particles. *J. Sed. Res.*, **23**, 117–119.
Rittenhouse, G. (1943) Relation of shape to the passage of grains through sieves. *Ind. Eng. Chem. Fundam.*, **15**, 153–155.
Rogers, C.S. (1990) Responses of coral reefs and reef organisms to sedimentation. *Mar. Ecol. Prog. Ser.*, **62**, 185–202.
Román-Sierra, J., **Muñoz-perez, J.J.** and **Navarro-Pons, M.** (2013) Influence of sieving time on the efficiency and accuracy of grain-size analysis of beach and dune sands. *Sedimentology*, **60**, 1484–1497.
Rouse, H. (1937) Modern conceptions of the mechanics or fluid turbulence. *Trans. Am. Soc. Civ. Eng.*, **102**, 463–505.
Rubin, D.M. (2004) A simple autocorrelation algorithm for determining grain size from digital images of sediment. *J. Sed. Res.*, **74**, 160–165.
Sadd, J.L. (1984) Sediment transport and $CaCO_3$ budget on a fringing reef, Cane Bay, St. Croix, U.S. Virgin Islands. *Bull. Mar. Sci.*, **35**, 221–238.
Savitzky, A. and **Golay, M.J.E.** (1964) Smoothing and differentiation of data by simplified least squares procedures. *Anal. Chem.*, **36**, 1627–1639.
Sayles, R.S. and **Thomas, T.R.** (1978) Surface topography as a non-stationary random process. *Nature*, **271**, 431–434.
Shields, A. (1936) *Application of Similarity Principles and Turbulence Research to Bedload Movement (English Translation of the original German manuscript).* Hydrodynamics Laboratory, California Institute of Technology, Pasadena, CA, USA.
Sime, L.C. and **Ferguson, R.I.** (2003) Information on grain sizes in gravel-bed rivers by automated image analysis. *J. Sediment. Res.*, **73**, 630–636.
Smith, D.A. and **Cheung, K.F.** (2002) Empirical relationships for grain size parameters of calcareous sand on Oahu, Hawaii. *J. Coastal Res.*, **18**, 82–93.
Sorby, H.C. (1879) The structure and origin of limestones. *Proc. Geol. Soc. London*, **35**, 56–95.
Smith, D.A. and **Cheung, K.F.** (2003) Settling characteristics of calcareous sand. *J. Hydraul. Eng.*, **129**, 479–483.
Stearn, C.W., **Scoffin, T.P.** and **Martindale, W.** (1977) Calcium carbonate budget of a fringing reef on the west coast of Barbados. *Bull. Mar. Sci.*, **27**, 479–510.
Storlazzi, C.D., **Norris, B.** and **Rosenberger, K.J.** (2015) The influence of grain size, grain color, and suspended-sediment concentration on light attenuation: why fine-grained terrestrial sediment is bad for coral reef ecosystems. *Coral Reefs*, **34**, 967–975.
Syvitski, J.P.M., **Smith, J.N.**, **Calabrese, E.A.** and **Boudreau, B.P.** (1988) Basin sedimentation and the growth of prograding deltas. *J. Geophys. Res.*, **93**, 6895–6908.
Warrick, J.A., **Rubin, D.M.**, **Ruggiero, P.**, **Harney, J.N.**, **Draut, A.E.** and **Buscombe, D.** (2009) Cobble cam: grain-size measurements of sand to boulder from digital photographs and autocorrelation analyses. *Earth Surf. Proc. Land.*, **34**, 1811–1821.
Yamano, H., **Miyajima, T.** and **Koike, I.** (2000) Importance of foraminifera for the formation and maintenance of a coral sand cay: Green Island, Australia. *Coral Reefs*, **19**, 51–58.

APPENDIX

Dietrich (1982) accounts for particle density, shape and roundness when converting particle size to settling velocity through three fitted equations (see Eq. 6) based on the non-dimensional settling velocity (W_*) and the non-dimensional grain size (D_*):

$$W_* = \frac{\rho w_s^3}{(\rho_{\text{part}} - \rho) g \upsilon} \quad (A1)$$

$$D_* = \frac{(\rho_{\text{part}} - \rho) g D_n^3}{\rho \upsilon^2} \quad (A2)$$

where ρ is fluid density, ρ_{part} is sediment density, v is kinematic viscosity, w_s is settling velocity and D_n is nominal diameter.

The three fitted equations in Eq. 6 account for particle size and density (*R1*), shape (*R2*) and roundness (*R3*). Particle size and density are related by a fourth-order polynomial:

$$R_1 = -3{\cdot}76715 + 1{\cdot}92944 \log D_* - 0{\cdot}09815 (\log D*)^2 - 0{\cdot}00575 (\log D*)^3 + 0{\cdot}00056 (\log D*)^4 \quad (A3)$$

Particle shape is accounted for via the Corey (1949) shape factor (CSF), which ranges from 0 to 1:

$$R_2 = \left(\log \left(1 - \frac{(1 - \text{CSF})}{0{\cdot}85} \right) \right) - (1 - \text{CSF})^{2{\cdot}3} \tanh(\log D_* - 4{\cdot}6) + 0{\cdot}3(0{\cdot}5 - \text{CSF})(1 - \text{CSF})^2 (\log D_* - 4{\cdot}6) \quad (A4)$$

Finally, the effect of particle roundness is incorporated using the Powers (1953) roundness index (PRI):

$$R_3 = \left[0{\cdot}65 - \left(\frac{\text{CSF}}{2{\cdot}83} \tanh(\log D_* - 4{\cdot}6) \right) \right]^{1+(3{\cdot}5-\text{PRI})/2{\cdot}5} \quad (A5)$$

These three equations are then combined to give w_s (Eq. 6).

Manuscript received 4 March 2016; revision accepted 18 October 2016